

Modeling Impact of Future Climate on Stability of Slope Based on General Circulation Model

S. Soralump¹ and T. Chaithong²

^{1,2}Department of Civil Engineering, Faculty of Engineering Kasetsart University, Bangkok, Thailand

¹E-mail: soralump_s@yahoo.com

ABSTRACT: Slope failures are one of geo-hazard which are one of the most dangerous and occur very often. Climate is an important role in stability of slope. In many cases rainfalls induce slope instability and lead to slope failure or landslide whereas evaporation might stabilize slope. Climate change due to greenhouse effect and global warming might affect precipitation and evaporation patterns in the future and influence future slope failure. Therefore, the paper proposes a method for assessment impact of climate change on slope failure occurrences based on general circulation model (GCM). Methodology combines between climate scenarios as a result of general circulation model and modified critical antecedent precipitation index model. GCM results are downscaled with dynamical-statistical technique to derive local climate. Analysis found that trends of susceptibility of soil instability vary and depend on climate in each year period.

KEYWORDS: Slope stability, Climate change, General circulation model, Landslides, Antecedent precipitation index

1. INTRODUCTION

Slope failures are significant geo-hazards which cause fatalities and properties damage. Economic cost loses more than hundred millions of dollars from 1979 to 2007 (Soralump, 2010). Landslide is natural phenomenon which occurred in the northern region of Thailand more than 15 times, resulted in over 280 deaths and over seventy millions of dollars of economic loss during 1970 to 2015. The number of landslides times in Thailand between 1970 and 2015 are shown in Figure 1.

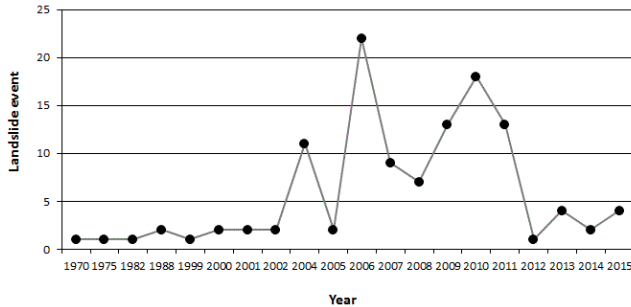


Figure 1 Number of landslides times in Thailand between 1970 and 2015

Climate is a key role in slope stability because it controls fluctuation of soil moisture or pore water pressure. Rainfall is one of climate factors and a major cause of the slope failures. The slope failures happen during or immediately after prolong rainfall and typhoon (Orence, 2004, Muntohar & Liao, 2010). The mechanism leading to rainfall-induced slope failures is well-understood. When rainwater infiltrates a ground and generates pore-water pressure. Increase in the pore-water pressure will reduce suction (negative pore-water pressure) and effective stress of the soil. Therefore, it affects decrease in shear strength on the failure plane. It leads to slope instability and slope failure. On the other hand, moisture leaves from the soil surface through the process of evaporation and will reduce the pore-water pressure but will increase the pore suction. It may stabilize the hillslope (Orence, 2004 Gasmu et al. , 2000, Chaithong & Soralump, 2015). Hence, prediction of future climate patterns is very useful for assessment the stability of slope.

The prediction of future climate patterns is simulated by general circulation models. General circulation models are type of complex climate model which represent physical processes of the atmosphere, ocean, and land surface. GCMs are successful in simulating of large-scale and long-term state of climate. However, GCMs have limitations in simulating the regional climate models (RCMs) due to their coarse horizontal resolution (about 300 × 300 km). Hence,

downscaling techniques are the process which downscale coarse horizontal resolution GCM outputs into finer horizontal resolution. The results of downscaling are called regional climate models which have horizontal resolution about 25x25 km. The downscaling techniques have two main approaches: dynamical and statistical downscaling techniques. (Buma & Dehn, 1998, 2000, Chinvano et al., 200, Ramirez-Villegas & Jarvis 2010; Tisseuil et al., 2010, Eisner et al., 2012, Chaithong & Soralump 2014, Chaithong 2015)

In the paper presents the combination of hydrological model based on GCM and landslide warning model for assessment risk of landslide occurrence in the future. This study uses a modified critical antecedent precipitation index model (MAPIcr) that exams the effect of future climate patterns on soil slope at Doi Pui , Chaing Mai, Thailand.

2. STUDY AREA AND METHODS

2.1 Study area and site investigation

The study area is residual soil slope at Doi Pui research station of Kasetsart University, Chiang Mai, Thailand. Figure 2 shows location of study area at Doi Pui Research Station. Soils at the study area are derived from the granite weathering rock. Land development department classified these soils into Doi-Pui soil series group. The soil profiles consisted of 1.75-m-thick decomposed granite rock overlain by 2.25-m-thick silty sand. The soil profiles were examined for physical and engineering properties by collected soil sample from boreholes drilled and test pit. Three boreholes were drilled until upper of decomposed granite rock and lower soil layers were investigated by standard penetration test until SPT value more than 50 blows per foot. Undisturbed soil samples were performed for each borehole. The test pit was excavated to a depth of 0.6 m for collection undisturbed soil samples. The undisturbed soil samples for test pit were taken by KU-Miniature sampler. The number of soil samples from test pit and boreholes were taken between 10 and 15. The soil samples were sheared by standard direct shear device for finding shear strength property. Table 1 shows soil properties of the study area. Figure 3 shows results of shearing tests.

The study area has a humid climate with average annual temperature about 20 °C and generally exceeds 30 °C during March to May (summer). The annual rainfall is 2,000 mm/year. Monthly precipitation shows a minimum between December and March, and a maximum precipitation in rainy season (August to September). Average annual evaporation rate is about 1,165 mm/year and monthly evaporation rate shows a maximum between February and May. Average relative humidity is between 56.7% and 89.3%, and wind speed is about 7.7 km/hr.(Jaithoeng 1997 and Chaithong and Soralump 2015)

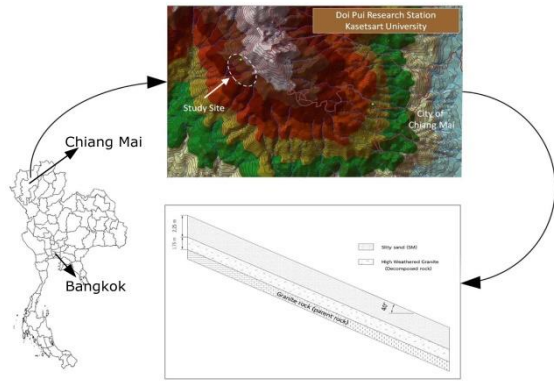


Figure 2 Location of study area at Doi Pui Research Station

Table 1 Soil properties of the study area

Property	Value
Plasticity index	5.5
Liquid limit	32.6
Dry density of soil (kN/m ³)	12.0
Saturated permeability, k _s (m/s)	6.903 x 10 ⁻⁷
Slope angle, (degree)	40
Unified Soil Classification System (USCS)	SM
Void ratio	0.776

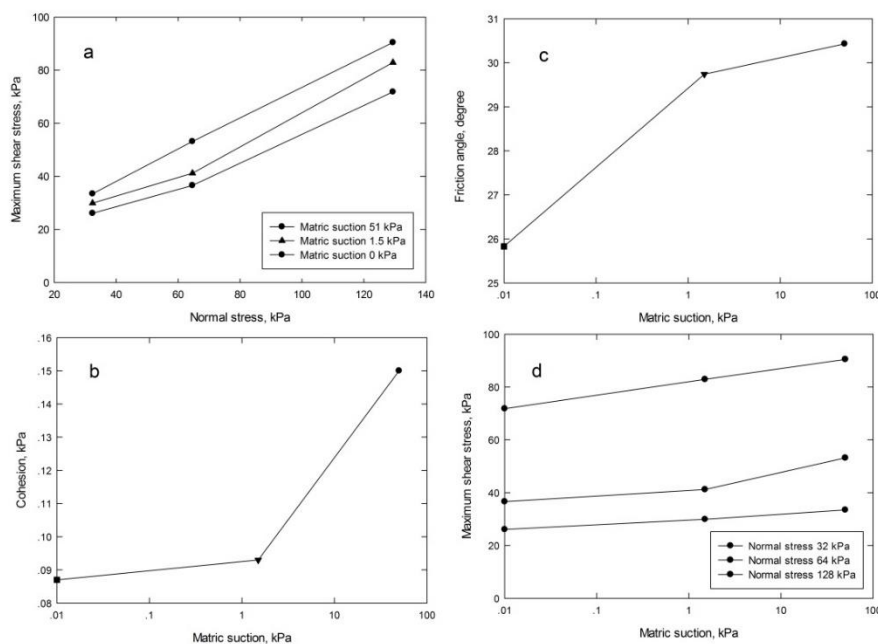


Figure 3 Devices used for determination of soil-water characteristic curve using tensiometer

In this study, soil – water characteristics curve (SWCC) is determined using miniature KU- tensiometer for metric suction 0 to 100 kPa. SWCC were tested an undisturbed soil sample that was collected from Doi Pui research station by KU-Miniature Sampler. First, the soil sample was trimmed to size with a PVC ring and was assembled on an aluminum base. Second, the samples were sealed to keep moisture evenly dispersed throughout the sample of approximately 24 - 48 hours. Next, soil sample was measured suction (initial soil matric suction) to balance by KU-tensiometer. The weighing, height and diameter of soil sample were measured to calculate moisture content. There are 2 paths of SWCC, drying path and wetting path. So, these studies begin from the drying path. The method is based on removing soil moisture by drying a soil sample about 1% - 2%. Then the samples are sealed to keep moisture evenly dispersed throughout the sample. After that measure matric suction to balance by KU-tensiometer include, weighing, height and diameter measurement to calculate moisture content. Repeat the method until soil matric suction about 80 kPa or bubble in the KU-tensiometer. The wetting path difference from drying path, add the moisture content of soil sample. At matric suction 0 kPa, the soil sample was soaked in the water about 24 – 48 hour, in order to make the soil sample was

fully saturated. Figure 4 shows devices used for determination of soil-water characteristic curve using tensiometer.

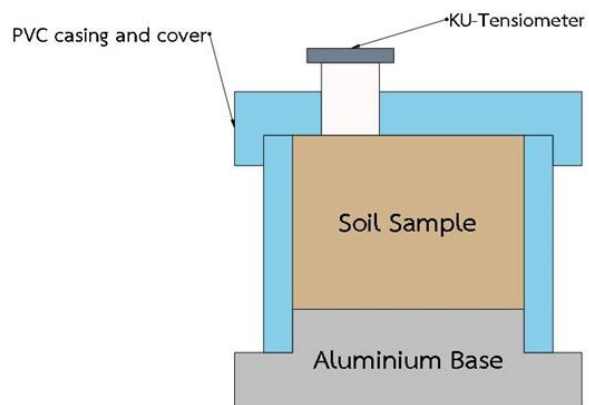


Figure 4 Devices used for determination of soil-water characteristic curve using tensiometer

2.2 Concepts of linkage general circulation model and landslide warning model

The methodology of assessment is combines the hydrological model as a result of GCM and the critical antecedent precipitation model. The hydrological model of research is an antecedent precipitation index based on GCM output. The antecedent precipitation index is used as input conditions for the critical API model. The assessment impact of climate change on stability of slope considers the following periods: 1. 1961-1990 (1970s, base year), 2. 2010-2039 (2020s, first future period), 3. 2040-2069 (2050s, second future period) and 4. 2070-2099 (2080s, third future period). Figure 5 shows concept of assessment impact of climate change on stability of slope.

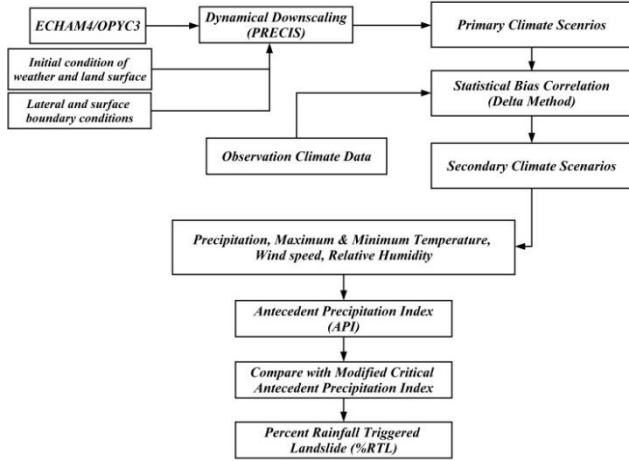


Figure 5 Concept of assessment impact of climate change on stability of slope

2.2.1 Climate change scenario

For the climate change scenario, this research used ECHAM4/OPYC3 of the Max-Plank institute for methodology in Hamburg, Germany. This research used emission scenario A2 because it is selected by National Research Council of Thailand for climate change research. The ECHAM4/OPYC3 has the horizontal resolution about $\sim 300 \times 300$ km ($\sim 2.8 \times 2.8$ degree). Southeast Asia START Regional Center (START) used dynamical downscaling technique for increase in the horizontal resolution of the ECHAM4/OPYC3. The horizontal resolution of the ECHAM4/OPYC3 increase from $\sim 300 \times 300$ km to $\sim 25 \times 25$ km. Results after downscaling are called a primary climate scenario (regional climate model). The primary climate scenario is still prone to biases with observations climate, hence, the statistical bias correction technique is used to adjust the biases of primary climate model. Equation 1 presents an equation for precipitation and wind speed. Equation 2 presents an equation for maximum and minimum temperature, and relative humidity.

$$x_{new} = x_{obs,base} * \left(\frac{x_{RCM, future}}{x_{RCM, base}} \right) \quad (1)$$

$$x_{new} = x_{obs,base} * \left(x_{RCM, future} - x_{RCM, base} \right) \quad (2)$$

where x_{new} is scenarios climate parameters after correction bias, $x_{obs,base}$ is observed climate parameters in base period, $x_{RCM, future}$ is RCM climate parameters in future period, and $x_{RCM, base}$ is RCM climate parameters in base period

Regarding to the Thiessen polygon analysis, it was found that the study area is under influence of Chiang Mai weather station. Therefore, the observation climates at Chiang Mai weather station (station code, 48327) during 1961 to 1990 are used to correct the biases of primary climate scenarios. The observation climates were investigated of reliability by double mass curve method. The investigation results found out that they passed investigation and are reliable to adjust the primary climate scenarios because all slope of double mass curves are straight line. Bias correction results are called secondary climate scenario and are used as input conditions of antecedent precipitation index. Moreover, this research used root mean square error (RMSE) for comparison results of before and after adjustment. The secondary climate scenario variables are calibrated with observation data during 2010 to 2015 for verification of correlation between simulation data and observation data. Equation 3 shows root mean square error equation. (Chaithong, 2015, and Chaithong & Soralump, 2016).

$$RMSE = \sqrt{\frac{1}{n} \sum (x_{obs} - x_{RCM})^2} \quad (3)$$

where $RMSE$ is root mean square error, x_{obs} is observed climate parameters, x_{RCM} is RCM climate parameters, n is number of day.

2.2.2 Antecedent precipitation index (API)

Basic concept of antecedent precipitation index is the accumulated moisture in ground at any time. The moisture in ground will rise due to rainfall but will decrease by time after the end of rainfall. Linsley et al., (1982) proposed an equation of API as shown in equation 4 (Thowiwat & Soralump 2009, 2010, Ohtsu et al., 2012).

$$API_t = (K_t \times API_{t-1}) + P_t \quad (4)$$

where API_t is the API on day 't' (mm), API_{t-1} is the API on day 't-1' (mm), K_t is recession constant, and P_t is rainfall on day 't' (mm).

Chodhury and Blanchard (1983) proposed the equation for recession constant calculation which is based on exponential function of daily evaporation and maximum soil moisture available for evaporation. The equation of recession constant shows in equation 5.

$$K_t = EXP(-E_t / W_m) \quad (5)$$

where E_t is evaporation on day 't' (mm) which is calculated by using Penman-Monteith equation, and W_m is maximum soil moisture available for evaporation (mm).

For this research, the evaporation for recession constant is calculated by using Penman-Wilson because the Penman-Monteith equation overestimates for actual evaporation calculation (Wilson, 1990). Hence, the equation of recession constant for this research shows in equation 6.

$$K_t = EXP(-AE_t / W_m) \quad (6)$$

where AE_t is actual evaporation on day 't' (mm) which is calculated by using Penman-Wilson equation. In addition to Eq. (6), we also have

$$AE_t = (\Gamma Q_n + \eta E_a) / (\Gamma + \eta / h_s) \quad (7)$$

where E_a is flux associated with mixing, h_s is relative humidity at the soil surface, Γ is slope of saturation vapor pressure versus temperature curve, Q_n is net radiation at the water surface,

mm/day, and η is psychrometric constant, kPa/°C, $\eta = 0.06733$ kPa/°C.

For this study, the maximum soil moisture available for evaporation can be found by evaporation experiment. The evaporation experiment was used two evaporation pans. Pan A filled with water and functioned as the reference pan for potential evaporation. Pan B contained the saturated undisturbed soil sample for measuring actual evaporation. Both pans were supported on sensitive weighing scales to monitor changes in mass. The tests were conducted under the room environment and dried by air dry. The relative humidity of the air above the evaporating surfaces was being recorded continuously throughout the test. Saturated undisturbed soil sample was prepared by soaking sample until the matric suction (negative pore water pressure) equal to 0 kPa. There are 4 testing of evaporation experiment. Figure 6 shows schematic of evaporation experiment.

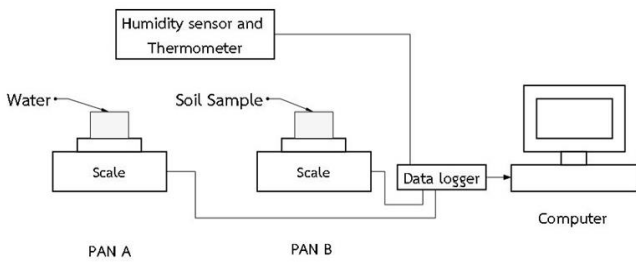


Figure 6 Schematic of evaporation experiment

2.2.3 Modified critical antecedent precipitation index model (MAPI_{cr})

The modified critical antecedent precipitation index model (MAPI_{cr}) is critical limit of moisture storage in ground for landslide warning. MAPI_{cr} developed from antecedent precipitation index in term of volume relationship of soil mechanics. Soralump (2007) proposed antecedent precipitation index based on function of degree of saturation, porosity, and critical thickness. When consider term of degree of saturation and porosity, found that degree of saturation at saturated condition multiply by porosity equal to volumetric water content as shown in equation 8.

$$\theta = n * Sr \tag{8}$$

where θ is volumetric water content, n is porosity, and Sr is degree of saturation

Antecedent precipitation index in term of volume relationship of soil mechanics shows in equation 9

$$API = n \times S_r \times T \tag{9}$$

where API is antecedent precipitation index, and T is thickness. Equation of the modified antecedent precipitation index shows in equation 10.

$$MAPI = \theta \times D \tag{10}$$

where $MAPI$ is modified antecedent precipitation index, and D is depth of soil (mm)

Hence, MAPI_{cr} is based on two simplifying assumption and function; volumetric water content at soaked state and critical depth. First, critical boundary of water storage in soil is the volumetric water content at soaked state. The volumetric water content at soaked state is taken from the SWCC at zero matric suction. Second, mechanism of slope failure is infinite slope, so the critical depth uses the infinite

slope model. Moreover the critical depth is the depth that gives factor of safety equal 1 at fully saturated state (matric suction equal to zero). Equation 11 shows the critical moisture threshold. Moreover, the critical depth is calculated by infinite slope model equation, which estimates using the Mohr–Coulomb failure criterion, as shown in equation 12.

$$MAPI_{cr} = \theta_s \times D_c \tag{11}$$

where $MAPI_{cr}$ is the modified critical antecedent precipitation index (mm), θ_s is the volumetric water content at soaked state, D_c is the critical depth, (mm).

$$FS = \frac{c + (\sigma_n - u_a) \tan \phi' + (u_a - u_w) \tan \phi^b}{\gamma_t z_w \sin \beta \cos \beta} \tag{12}$$

where FS is factor of safety, c is cohesion of soil, $(\sigma_n - u_a)$ is net normal stress, $(u_a - u_w)$ is matric suction, ϕ' is friction angle, ϕ^b is Angle indicating the rate of increase in shear strength relative to a change in matric suction, γ_t is density of soil, z_w is depth of soil, and β is slope angle.

Analysis level of susceptibility of slope failure use percent rainfall triggered landslide (RTL%) as shown in Table 2. S. Soralump (2014) proposed the percent rainfall triggered landslide based on relationship of antecedent precipitation index and critical antecedent precipitation model as shown in Table 2. This research use equation 13 for rainfall triggered landslide calculation.

$$RTL = (API_t / MAPI_{cr}) * 100 \tag{13}$$

where RTL is percent of rainfall triggered landslides

Table 2 Index of percent rainfall triggered landslide (based on slope gradient 25 degree)

Factor of safety	RTL, %	Definition of landslides susceptibility
< 1.1	> 55	Very high
1.1 – 1.3	55 - 35	High
1.3 – 1.5	35 - 20	Medium
> 1.5	< 20	Low

3. RESULTS AND DISCUSSION

3.1 Evaporation experiment results and recession constant

According to the evaporation testing, they showed that average maximum soil moisture available for evaporation is 18.13 mm. Figure 7 shows plots the actual evaporation versus drying time for test no. 1, 2, 3 and 4. Variations of recession constant depend on the changing of actual evaporation rate, such as, April displays the highest rate of actual evaporation which leads to the lowest of the recession constant, in contrast, January displays the lowest rate of actual evaporation which leads to the highest of the recession constant. Figure 8 shows average expected monthly evaporation. When consideration of increase in expected actual evaporation in the future, they influence to decrease in recession constant in each period which differ with the recession constant of department of water resource (DWR) because the recession constant of DWR content values in each month as shown in Table 3. Therefore, the recession constant can be in form to five groups as shown in Figure 9.

The comparison between the recession constant of DWR and the recession constant of this study found that the recession constant of DWR less than the recession constant of this study. The recession constant of this study have the value approximately 0.925 and 0.87 but the recession constant of DWR have the value approximately 0.7 and 0.8. As a result, there will be the difference between the API that using the recession constant of DWR and the API that using the recession constant of this study. The API that using the recession constant of this study have the value more than the antecedent precipitation index that using the recession constant of DWR. Moreover, the recession constant of this research vary that depend on change of actual evaporation in each year.

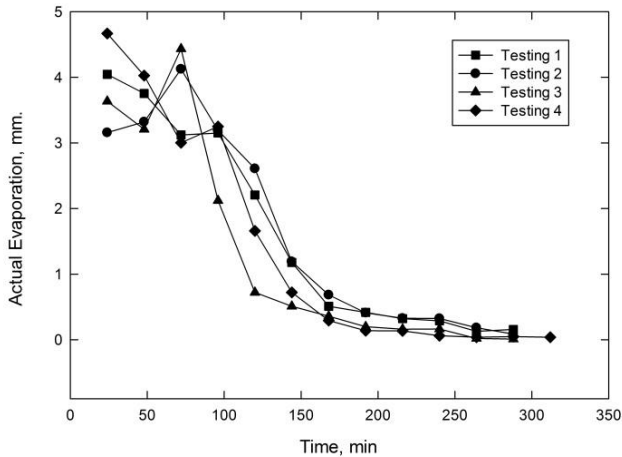


Figure 7 Actual evaporation versus drying time for test no. 1, 2, 3 and 4

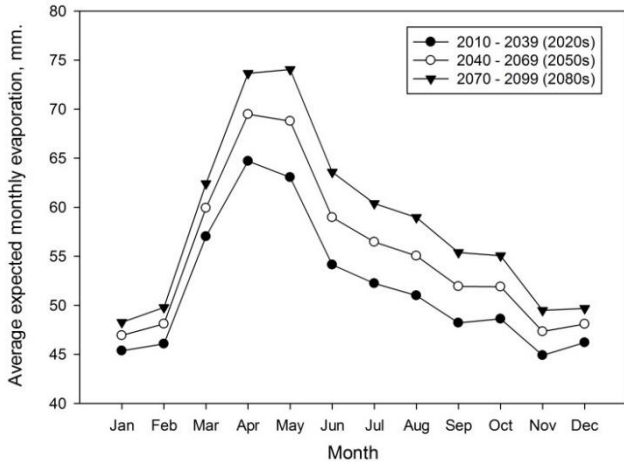


Figure 8 Average expected monthly evaporation

Table 3 Monthly recession constant values of department of water resource (DWR)

Month	Recession constant	Month	Recession constant
January	0.727	July	0.793
February	0.746	August	0.801
March	0.720	September	0.800
April	0.728	October	0.794
May	0.749	November	0.765
June	0.789	December	0.746

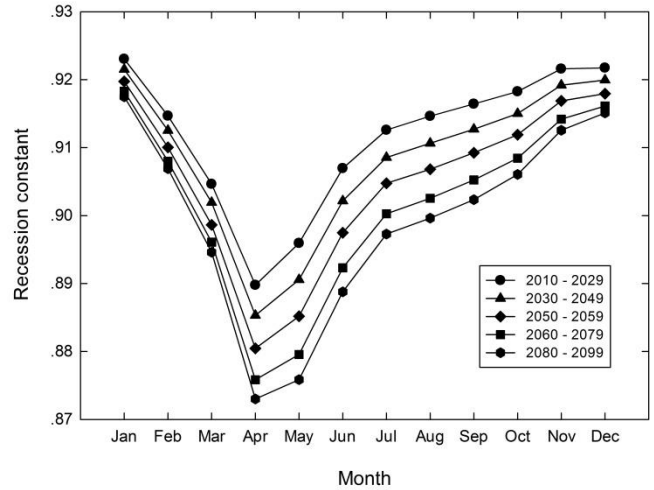


Figure 9 the recession constants

3.2 Future Climate Scenario and Antecedent Precipitation Index

Consideration about results of adjustment bias of primary climate scenario shows in Table 4. The root mean square error of all climate parameters is fall after correction the bias of primary climate scenario. The root mean square is decrease of 6.78% for precipitation; 28.64% for maximum temperature; 37.60% for minimum temperature; 24.40% for wind speed. Therefore, the secondary climate scenario has a good correlation with the observation data more than primary climate scenario.

Future average annual maximum temperature will rise approximately 0.35°C per decade and average annual minimum temperature will rise approximately 0.6° C per decade. The expected annual precipitation trend will fall gradually during 2020s to 2050s and will rise slightly for the last 30 years of this century but insignificant of change when, compare with base period as shown in Figure 10. The expected wind speed trend remains steadily over the period. Average annual relative humidity will fall approximately 1.2 % per decade. The expected actual evaporation will increase of 1.6 mm. per year. Figure 11 shows the average annual precipitations between 2010 and 2099. Figure 12 shows the average annual maximum temperature and the average annual minimum temperature between 2010 and 2099. Figure 13 shows the actual evaporation between 2010 and 2099.

Expected antecedent precipitations will decline about 1.85% per decade as a result of rise in the actual evaporation rate. The expected antecedent precipitations reach a peak in 2010, 2016, 2036, 2040, 2046, 2066, 2070, 2076, and 2096 which are exceed 250 mm. Figure 14 shows the expected the antecedent precipitation index between 2010 and 2099.

Table 4 Root mean square error (RMSE) for before and after correction

Climate parameter	Before correction (primary climate scenario)	After correction (secondary climate scenario)
Precipitation	1.18	1.10
Maximum temperature	4.40	3.14
Minimum temperature	3.91	2.44
Wind speed	4.96	3.75

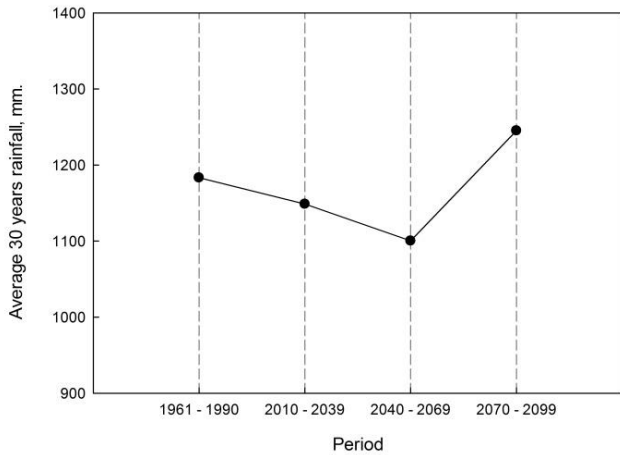


Figure 10 Average 30 year rainfall

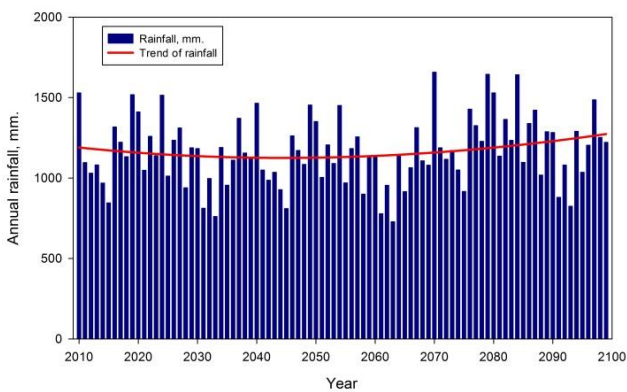


Figure 11 Average annual precipitations between 2010 and 2099

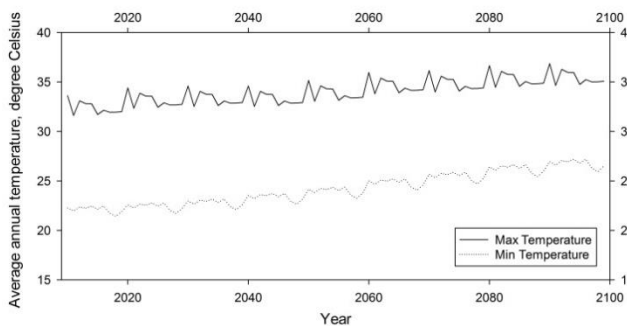


Figure 12 Average annual maximum temperature and the average annual minimum temperature between 2010 and 2099

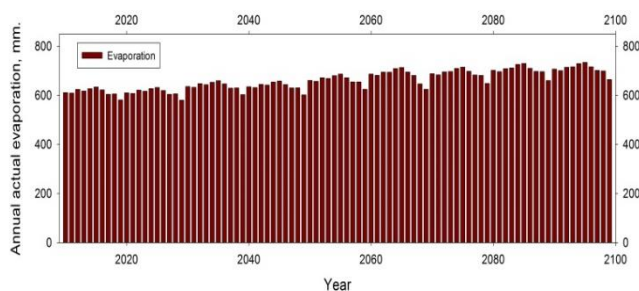


Figure 13 Actual evaporation between 2010 and 2099

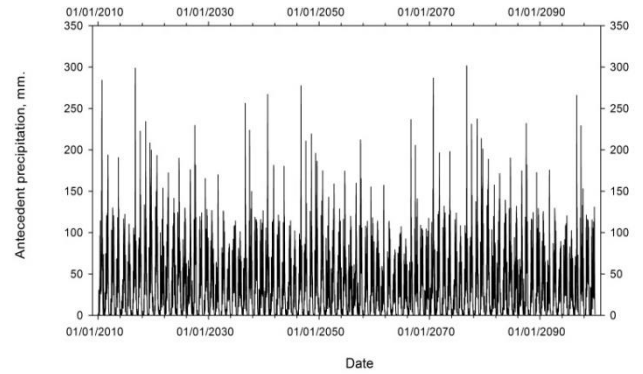


Figure 14 Antecedent precipitation index between 2010 and 2099

3.3 Susceptibility of slope failure

The critical depth of critical moisture threshold is the depth that gives a factor of safety equal to 1 that used infinite slope model as shown in equation 12, and parameters as shown in Table 1 and Figure 2. The results of calculation found that the critical depth for this research is 2.0 m. The slope angle for critical depth calculation only used single slope angle where was investigated soil physical and engineering properties. Figure 15 shows the factor of safety versus depth. The volumetric water content at soak state is 43.4%, is also taken from soil-water curve characteristic curve at zero suction as shown in Figure 16. Hence, the modified critical antecedent precipitation index is 875 mm.

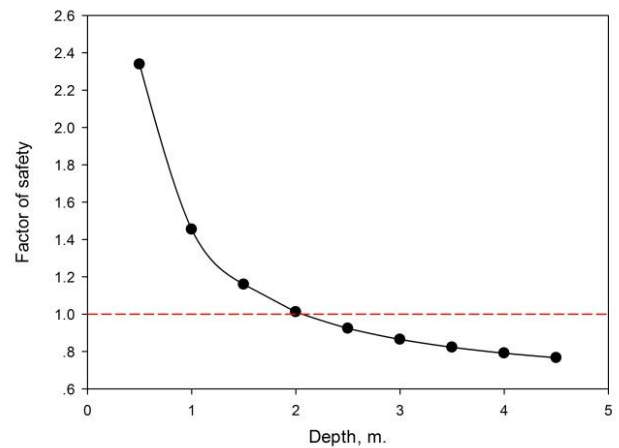


Figure 15 Factor of safety versus depth

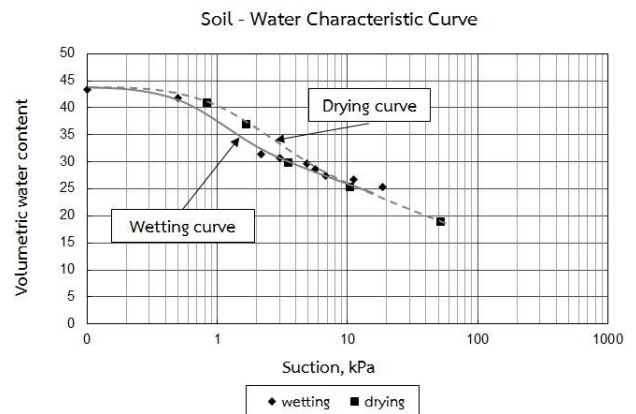


Figure 16 Soil-water characteristic curves

Considering the difference between RTL of observation data at Doi Pui and RTL of RCM, it was found that the trend of RTL of RCM is quite agree with the trend of RTL of observation. Moreover, the RTL of observation is over more than the RTL of RCM. Figure 17 show the RTL of observation data at study site and the RTL of RCM. The RMSE of RTL of observation and RCM is 4.79.

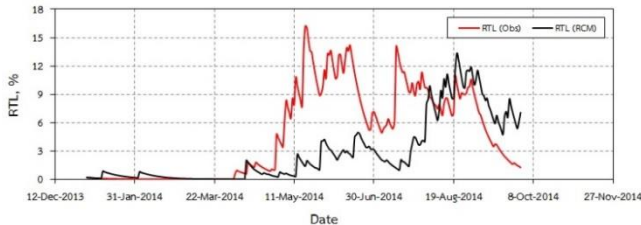


Figure 17 RTL of observation data at study area and RCM

The prediction of rainfall triggered landslide based on the ECHAM4/OYPC3 and critical moisture threshold found that number of days, which has RTL value less than < 20% (low susceptibility), increases by 0.12% for 2020s, 0.33% for 2050s and 0.17% for 2080s from the analysis of the base year (1961-1990). For medium susceptibility of slope failure occurrence (RTL during 20% to 35%), the number of days falls by 14.6% for 2020s, 42.7% for 2050s, and 21.2% for 2080s which compares the base year. Moreover, the number of days which has the high susceptibility of slope failure occurrence (RTL during 35 % to 55%) remains steady over the period. Figure 16 shows the prediction of susceptibility of slope failure occurrence.

According to analysis trend of susceptibility of slope failure, it found that the stability of study slope is increase in the first future period (2020s) and the second future period (2050s) but decrease in the third future period (2080s) as shown in Figure 18, and the trend is correlation with the trend of future precipitation as shown in Figure 10. Moreover, consider the expected rainfall in 2080s found that it is more than rainfall in base period (1970s), but the susceptibility of slope failure of 2080s more than base period (1970s) due to effect of increment of actual evaporation. The increment of actual evaporation affects increase in recession constant and decrease in API.

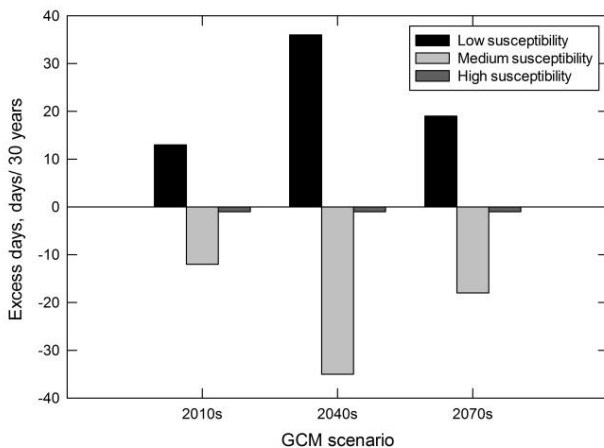


Figure 18 Prediction of susceptibility of slope failure occurrence

4. CONCLUSION

Simulation of impact of climate change on slope stability based on ECHAM4/OYPC3 and critical moisture threshold. The results found from this study could be concluded:

The trend of susceptibility of landslide is downward during the first 60 years (between 2020s and 2050s) but an upward trend of susceptibility of landslide occur during the last 30 years 10 (2080s).

Considering last 30 year (2080s), it was found that the rainfall is more than the base year, 2020s and 2050s but the excess days is quite similar 2020s because the effect of evaporation increasing. Therefore, the characteristic of future rainfall is a significant role in control the trend of susceptibility of slope failure. Changing evaporation affects antecedent precipitation in ground which influences trend of susceptibility of slope failure.

5. ACKNOWLEDGEMENTS

The authors would like to acknowledge the Southeast Asia START Regional Center for providing the regional climate model and also the Thai meteorological department for patronage the meteorological data, and gratefully thank you department of mineral resource of Thailand and Geotechnical Engineering Research and Development Center (GERD) for support field and site investigation. The authors would sincerely like to thank Asst. Prof. Dr. Apinit Jotisankasa, Asst. Prof. Dr. Jirawat Ganasut and geotechnical innovation laboratory for equipment and suggestion.

6. REFERENCES

Buma, J., and Dehn M., (1998) A method for predicting the impact of climate change on slope stability. *Environmental Geology* 35: 190-196

Chaithong, T., (2015) Investigation of evaporation effect on soil slope stability in relation to climate change. Master thesis, Kasetsart University

Chaithong, T., and Soralump S., (2014) The Potential Impacts of Climate Change on Landslide Triggering. EIT-JSCE Joint International Symposium on International Human Resource Development for Disaster-Resilient Countries 2014, Thailand

Chaithong, T., and Soralump S., (2015) The effects of evaporation flux boundary condition on pore water pressure in hillslope. The 20th National Convention on Civil Engineering, 8-10 July, Chonburi, Thailand

Chaithong T., and Soralump S., (2016) Statistical bias correction technique for precipitation data output of global climate circulation under emission scenarios A2 and B2. *The Journal of KMUTNB.*, vol. 26, no. 2 (In Thai)

Chinvanno, S., Laung-Aram V., Sangmanee C., and Thanakitmetavut J., (2009) Future climate projection for Thailand and Mainland Southeast Asia using PRECIS and ECHAM4 climate models. Southeast Asia START Regional Center Technical Report, no. 18

Eisner, S., Voss, F., and Kynast, E., (2012) Statistical bias correction of global climate projections-consequences for large scale modeling of flood flows. *Advances in Geosciences* 31:75-82 doi:10.5194/adgeo-31-75-2012

Gasmo, JM., Rahardjo, H., Leong, EC., (2000) Infiltration effects on stability of a residual soil slope. *Computers and Geotechnics* 26:145-165

Jaithoeng, A., (1997) Site Improvement at Suan Song – Saen, Doi Pui Station Changwat Chiang Mi as Tourist Attraction. Master thesis, Kasetsart University (In Thai)

Muntohar, AS., and Liao, HJ., (2010) Rainfall infiltration: infinite slope model for landslides triggering by rainstorm. *Nat Hazards* 54:967-984 doi: 10.1007/s11069-010-9518-5

Orense, RP., (2004) Slope Failures Triggered by Heavy Rainfall. *PHILIPPINE ENGINEERING JOURNAL* Vol. 25 No. 2:73-90

Ramirez-Villegas, J., and Jarvis, A., (2010) Downscaling global circulation model outputs: the delta method decision and policy analysis working paper No. 1. International Center for Tropical Agriculture

Soralump, S., (2007) Development of Landslide Hazard Mapping in Thailand. A National Training Course on Landslide Risk Management, 17-19 October, Ridgewood Residence, Bangui City, Philippines

- Soralump, S., (2010) Geotechnical Approach for the Warning of Rainfall-Triggered Landslide in Thailand Considering Antecedence Rainfall Data, proceeding of International Conference on Slope 2010 : Geotechnique and Geosynthetics for Slopes, Chiang Mai, Thailand.
- Thowiwat, W., and Soralump, S., (2009) Critical API Model for Landslide Warning. The 14th National Convention on Civil Engineering, Nakhon Ratchasima, Thailand (In Thai)
- Thowiwat, W., and Soralump, S., (2010) Critical API Model for Landslide Warning. The 15th National Convention on Civil Engineering, Ubon Ratchathani, Thailand (In Thai)
- Tisseuil, C., Vrac, M., Lek, S., and Wade, A.J., (2010) Statistical downscaling of river flows. *Journal of Hydrology*, vol. 385: 279–291 doi:10.1016/j.jhydrol.2010.02.030
- Ohtsu, H., Chaleiwchalard, N., Koga, H., and Soralump, S., (2012) A study on landslide early warning system considering the effect of antecedent rainfall on slope stability.